Electromagnetic Compatibility in Electron Cyclotron Resonance Heating System

Weiye Xu, *Member, IEEE*, Handong Xu, Fukun Liu, Huaichuan Hu, and Jianqiang Feng

***Abstract*— The electron cyclotron resonance heating (ECRH) is a very important plasma heating method in experimental advanced superconducting tokamak (EAST). There are four gyrotrons in the EAST ECRH system that can generate 4-MW/100-s/0.14-THz wave. The ECRH system is a complex terahertz system that involves ultralow temperature, ultrahigh vacuum, strong magnetic field, high-power electromagnetic wave, and weak diagnostic signal. There are many electromagnetic compatibility problems in the ECRH system. This is the first report about the electromagnetic compatibility for the ECRH system. In the operation of the ECRH system, many electromagnetic compatibility problems have been found and resolved. We can suppress the interference and improve the accuracy of power monitoring and the effectiveness of radio frequency protection by using the magnetic rings. The influence of the magnetic field on the current transformers was analyzed. Some electromagnetic compatibility issues in the data acquisition system were discussed. After solving the electromagnetic compatibility problems, the EAST ECRH system can stably output high-power terahertz wave.**

***Index Terms*— Electromagnetic compatibility, electron cyclotron resonance heating (ECRH), power monitoring, terahertz system.**

I. Introduction

THE electron cyclotron resonance heating (ECRH) is a very important plasma heating method in experimental advanced superconducting tokamak (EAST) [1], [2] for nuclear fusion research [3] in the Institute of Plasma Physics, Chinese Academy of Sciences, Hefei, China. The gyrotrons [4]–[6] are widely used as the millimeter-wave or terahertz sources for the ECRH system. There are four gyrotrons in the EAST ECRH system. Each gyrotron can generate 1-MW/100-s/0.14-THz wave [7]. In the experiments in recent years, the #1 gyrotron oscillation of 903 kW/10 s, 834 kW/95 s, and 650 kW/754 s were achieved, the #2 gyrotron oscillation of 647 kW/2 s, 499 kW/80 s, and 406 kW/98 s were achieved, and the #3 gyrotron oscillation of 787 kW/20 s, 637 kW/100 s, and 559 kW/1000 s were achieved. The output radio frequency (RF) power was measured using the calorimetric method [8].

Manuscript received August 21, 2018; revised October 19, 2018 and November 8, 2018; accepted December 4, 2018. Date of publication December 18, 2018; date of current version May 8, 2019. This work was supported in part by the National Key Research and Development Program of China under Grant 2017YFE0300401 and in part by the National Magnetic Confinement Fusion Science Program of China under Grant 2015GB102003 and Grant 2015GB103000. The review of this paper was arranged by Senior Editor P. K. Chu. *(Corresponding authors: Weiye Xu; Handong Xu.)*

The authors are with the Institute of Plasma Physics, Chinese Academy of Sciences, Hefei 230031, China (e-mail: xuweiye@ipp.cas.cn; xhd@ipp.cas.cn).

Color versions of one or more of the figures in this paper are available online at http://ieeexplore.ieee.org.

Digital Object Identifier 10.1109/TPS.2018.2885400

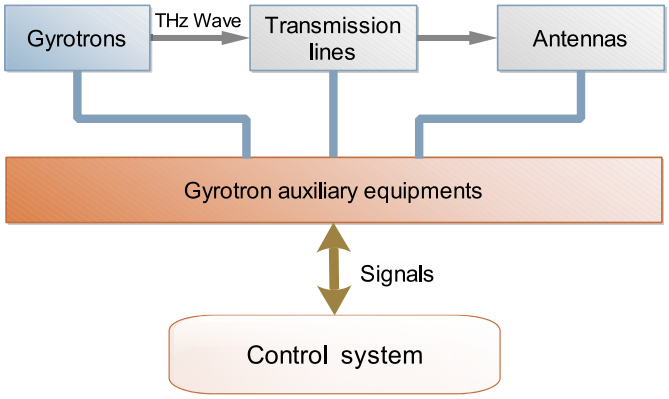

Fig. 1. Architecture of the EAST ECRH system.

The ECRH system is a complex terahertz system that involves ultralow temperature, ultrahigh vacuum, strong magnetic field, high-power electromagnetic wave, and weak diagnostic signal. There are many electromagnetic compatibility problems inside the system, and there are many electromagnetic interference (EMI) problems outside the system. We can see that there are many reports [3], [9], [10] on the ECRH system, which is a complex electromagnetic system. However, there is no detailed report on the electromagnetic compatibility of the ECRH system. Solving the electromagnetic compatibility problems is related to the successful operation of the ECRH system. In the operation of the EAST ECRH system, many electromagnetic compatibility problems have been found and resolved, and they were analyzed and discussed in this paper.

II. ECRH System on EAST

The EAST ECRH system is designed to output 4-MW/100–1000-s/0.14-THz wave power. The terahertz generator (gyrotron) is the most important device in the ECRH system. The architecture of the ECRH system is shown in Fig. 1. The ECRH system can be divided into three layers. The first layer includes the gyrotrons, the transmission lines, and the antennas. The second layer is the gyrotron auxiliary equipment layer. The gyrotron auxiliary equipments include the superconducting magnet and its power supply, the ion pump power supply, the cathode high-voltage power

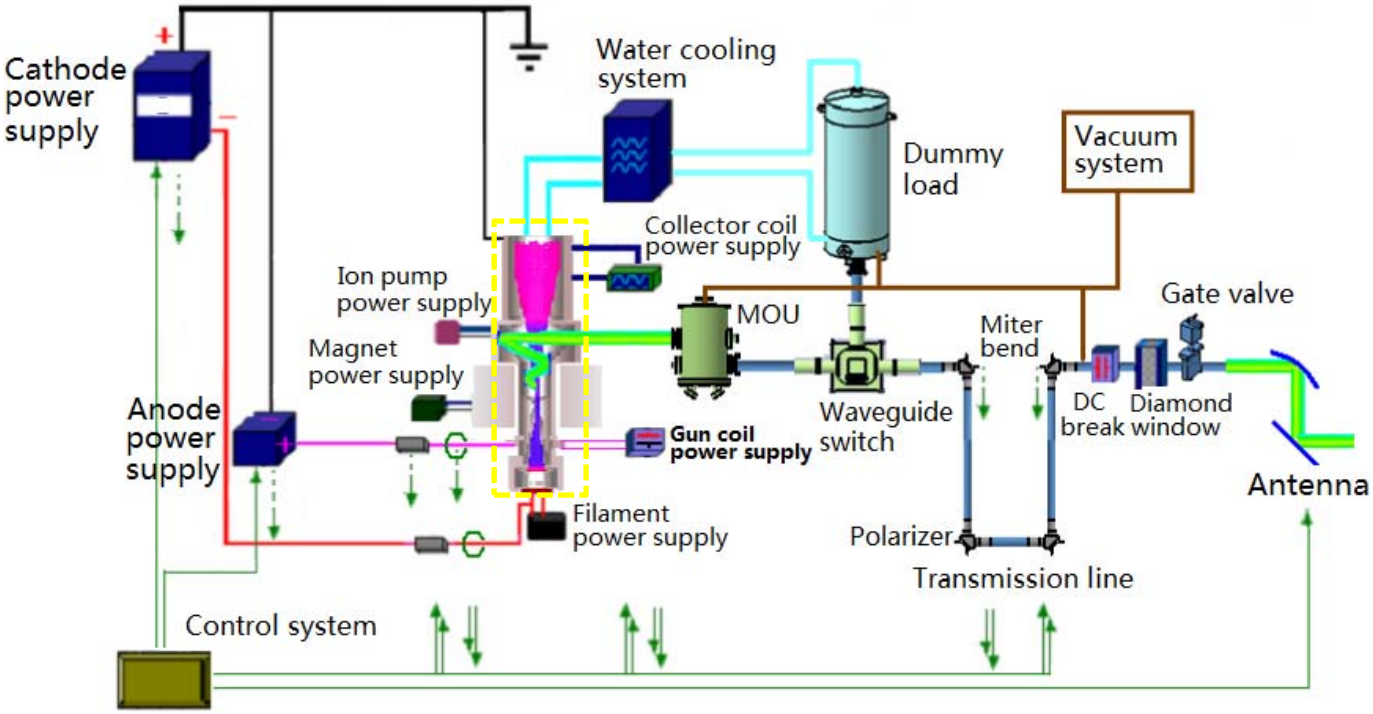

Fig. 2. Schematic of the EAST ECRH system. Only one system is drawn in this image, and the other three systems have the same structure. Yellow dashed rectangle: gyrotron.

supply, the anode high-voltage power supply, the water cooling system, the vacuum system, and the cryogenic system. All these auxiliary devices are shown in Fig. 2. The third layer is the control system. The control system consists of the central timing controller, the RF protection and power monitoring system [11], the interlock system, the overcurrent protection system, the arc protection system, the data acquisition (DAQ) system, the polarization control system, and the video monitoring system. The signal connection diagram of the control system is shown in Fig. 3. The control system shown in Fig. 3 was designed for two gyrotrons. Two gyrotrons share one cathode high-voltage power supply. There are two sets of identical control systems for four gyrotrons in EAST ECRH system. Except that the interlock system and the DAQ system are shared by four gyrotrons, all the other equipments are shared by two gyrotrons.

III. Electromagnetic Compatibility in the RF Protection System for the Gyrotrons

The RF protection system is an important subsystem for gyrotrons. It is designed to realize the RF protection and to monitor the wave power in real time.

The electromagnetic environment is very harsh due to the ECRH system is close to the EAST tokamak, the lower hybrid current drive system (using the klystrons as the microwave sources) [12], the ion cyclotron range of frequencies (ICRF) system (using the tetrodes as the RF sources), and the high-voltage power supplies. Because the detector output signal is small (generally less than 1 mV) for gyrotron power monitoring [11], it is particularly susceptible to EMI, especially susceptible to the EMI generated by the ICRF system (with the frequency of 25–70 MHz) [13].

In addition, the anode voltage (body voltage) and the ion pump current signals are also seriously interfered. Fig. 4 shows the interference of the reflected wave detection voltage, the anode voltage, and the ion pump current during the operation of the ICRF system. It can be seen that when the ion cyclotron wave is generated, the above three signals are severely distorted and are unable to represent true values.

The interferences of the anode voltage and the ion pump current signals were easily suppressed by replacing the well-shielded chassis.

The interference of the diode detector signal is more complicated. We carried out detailed tests and found that the interference of the diode detector signal is generated by the diode detector, but not the attenuator or the amplifier. The diode detector may be influenced by the EMI by two ways shown in Fig. 5. One way is through the input port of the detector (through the horn antenna). The second way is through the output port of the detector (through the output coaxial line).

Let us first analyze the first possible coupling path. The horn antenna is followed by a WR6 rectangular waveguide with a cutoff frequency of 90.8 GHz and a length of approximately 1 cm. Since the EMI frequency (25–70 MHz) is less than the cutoff frequency, we need to analyze the attenuation of the rectangular waveguide in this case.

The electromagnetic field can be expressed as

$$\boldsymbol{E} = \boldsymbol{E_m} e^{j(\omega t - \beta z)} \tag{1}$$

$$\boldsymbol{H} = \boldsymbol{H_m} e^{j(\omega t - \beta z)}. \tag{2}$$

where E represents the electric field strength, E_m represents the amplitude of the electric field, H represents the magnetic field strength, and H_m represents the amplitude of

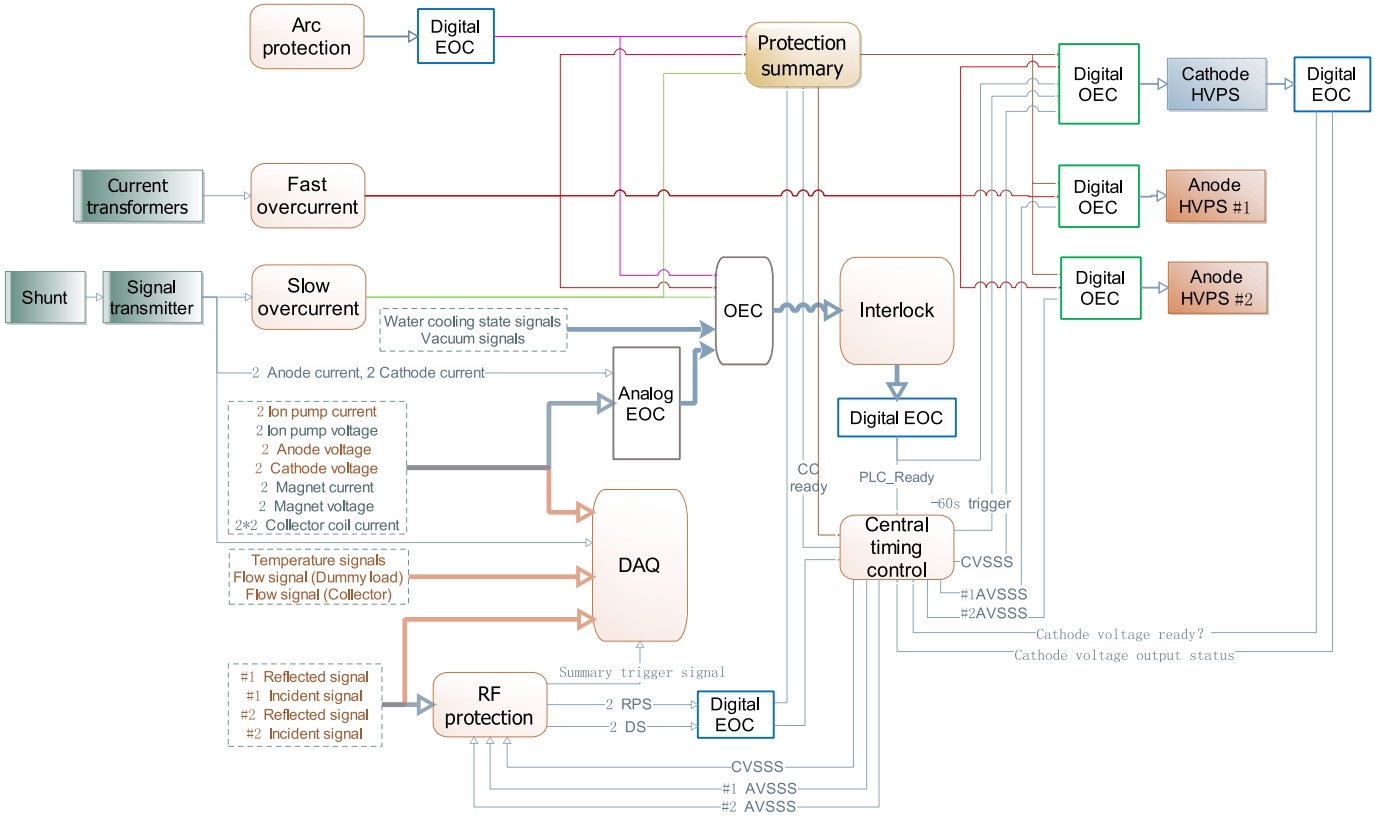

Fig. 3. Signal connection diagram of the control system. Hollow arrow line: electric signal and solid arrow line: light signal. The number "2" in front of the signal name indicates that there are two signals in total. CC: central controller, HVPS: high-voltage power supply, EOC: electrooptical conversion, PEC: optical-electrical conversion, DAQ: data acquisition, RPS: reflection protection signal, DS: disruption signal, CVSSS: cathode voltage start and stop signal, and AVSSS: anode voltage start and stop signal.

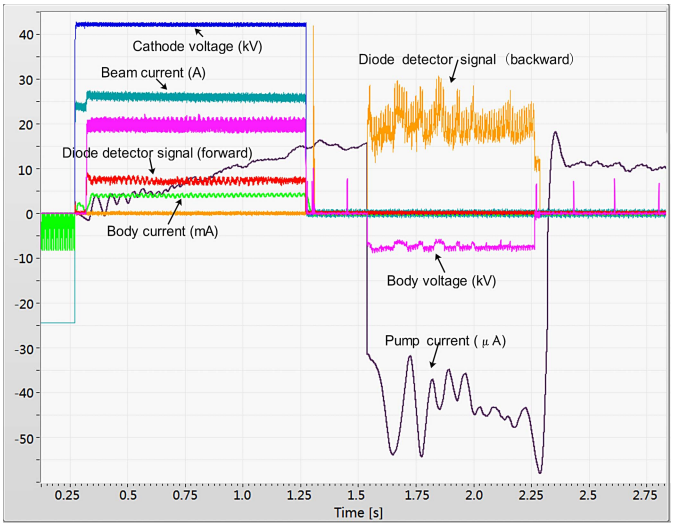

Fig. 4. Interference of the diode detector output voltage for the reflected wave, the anode voltage, and the ion pump current during the operation of the ICRF system.

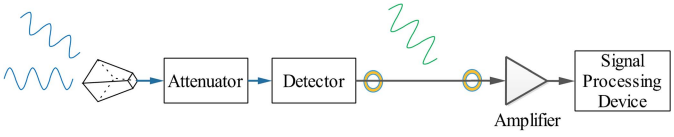

Fig. 5. Two ways to bring the EMI into the detector.

the magnetic field. The propagation constant is

$$\beta = \sqrt{\mu\varepsilon\left(\omega^2 - \omega_c^2\right)}. \tag{3}$$

where $\omega = 2\pi f$ represents the transmission angular frequency and $\omega_c = 2\pi f_c$ represents the cutoff angular frequency. When the transmission frequency is less than the cutoff frequency, i.e., $\omega < \omega_c$

$$\beta_{cc} = \pm j\alpha = \pm j\sqrt{\mu\varepsilon}\left(\omega_c^2 - \omega^2\right). \tag{4}$$

When the above formula takes "+," the propagation factor $e^{-j\beta z}$ becomes the growth factor $e^{-j\beta_{cc}z} = e^{\alpha z}$. Because there is no other excitation source, there is no way to keep the field increasing. When the above formula takes "−," the propagation factor $e^{-j\beta z}$ becomes the attenuation factor $e^{-j\beta_{cc}z} = e^{-\alpha z}$, which is reasonable.

For WR6 waveguides, the cutoff frequency is

$$f_c = 90.8 \text{ GHz}. \tag{5}$$

When the transmission frequency is $f = 2570$ MHz, the field strength attenuation factor is

$$\alpha_M = 2\pi\sqrt{\mu\varepsilon\left(f_c^2 - f^2\right)} = \frac{2\pi}{c}\sqrt{\left(f_c^2 - f^2\right)} \approx \frac{2\pi}{c} f_c \approx 1901.7 \text{ (Np/m)}. \tag{6}$$

Therefore, the corresponding power attenuation factor is

$$\alpha_{pM} = 2\alpha_M = 4\pi\sqrt{\mu\varepsilon\left(f_c^2 - f^2\right)} \approx \frac{4\pi}{c} f_c \approx 3803.4 \text{ (Np/m)}. \tag{7}$$

Assume that the incident power is P_i, then after the distance z, the remaining power is

$$P_{ri} = P_i e^{-\alpha_{\mathrm{pM}} z} = P_i e^{-3803.4z}. \quad (8)$$

Since the length of the waveguide is about 1 cm

$$P_{ri} = P_i e^{-3803.4\times 0.01} = P_i e^{-38.034} \approx 3P_i \times 10^{-17}. \quad (9)$$

Even if the EMI power coupled to the waveguide is 100 W (which is impossible), the power delivered to the detector is $3\times 10^{-15} W = 3$ fW. This power is very small, so this coupling path can be ignored.

In order to verify the above analysis, we installed a shielded box with an internal absorbing material outside the power monitor bend. The test results show that the interference voltage caused by the ICRF wave to the detector voltage is similar to the previous one. It proves that the first coupling path can be ignored.

The second possible coupling path is the output coaxial line. In order to prevent the ground bounce from causing damage to the detector, the detector and amplifier are floating. That is, the outer shield of the coaxial line that is used as the signal negative wire is floating. The line length is about twenty meters, which is close to the ICRF wavelength (4.29–12 m). The ungrounded coaxial line becomes an ICRF receiving antenna, which couples the ICRF wave into the detector. The detector outputs a video signal related to the received ICRF wave power, and floods the voltage signal generated by the ECRH wave power.

In order to suppress the coupling of the second way, one solution is to use a shielded twisted pair instead of a coaxial line. The signal positive pole and the negative pole are connected to two core wires, and the shield layer is grounded. In the short distance case, the shielding effect of the double-ended grounding is better than the single-ended grounding. When the signal line length is very long, the potential of the two grounding points may be different. If the two ends are grounded, the shielding layer will form a ground potential difference. The induced current, on the other hand, interferes with the signal, so in this case, single-ended grounding is generally adopted, but single-ended grounding only has a good shielding effect for the line length $L \ll \lambda$. The above analysis is in the case where the shielding layer can be ideally shielded. In actual cases, the shielding is not ideal. The experimental results show that when the shielded twisted pair is used; the detector signal is even worse, as shown in Fig. 6. It is because the shielding is not good; the external EMI causes almost the same common mode interference on two symmetrical core lines. When the shield layer is connected to the negative core wire (signal line), the positive and negative signal lines are no longer symmetrical, and the common mode interference is significantly reduced, which is shown in Fig. 7. It can be seen that this solution is not very good.

Another solution to suppress the coupling of the coaxial line is adding a magnetic ring at both ends of the coaxial line to filter out the high-frequency signals. The magnetic ring for EMI suppression mainly includes MnZn and NiZn materials. The MnZn is mainly used for low-frequency (hundreds of kilohertz to several tens of megahertz) interference suppression.

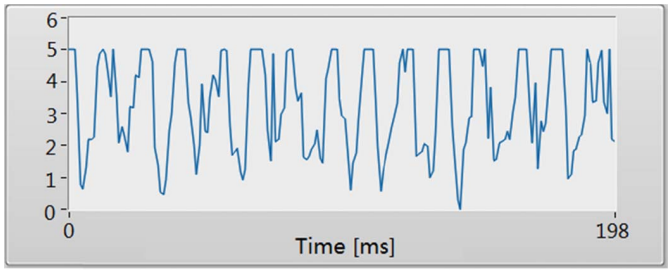

Fig. 6. Detector output voltage signal when the shielded twisted pair (the shield is grounded) is used between the detector and the amplifier.

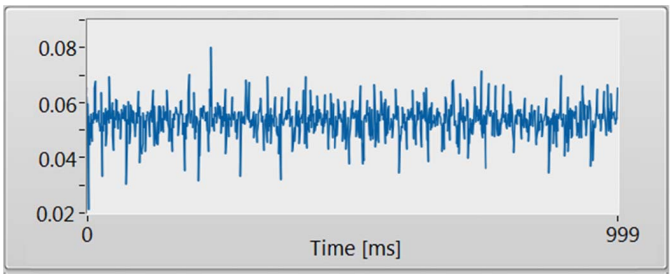

Fig. 7. Detector output voltage signal when the shielded twisted pair (the shield is connected to the negative signal core wire) is used between the detector and the amplifier.

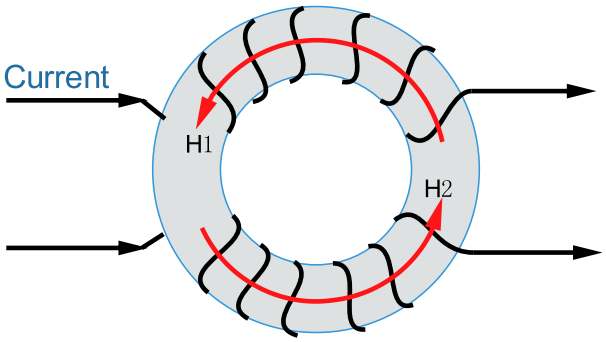

Fig. 8. General structure of the common mode choke.

The NiZn is mainly used for high-frequency (1 MHz to several gigahertzes) interference suppression. The magnetic ring we use is made of NiZn 4W620 material with a magnetic permeability of about 620. It has good impedance characteristics for the ICRF band (25–70 MHz).

The common mode choke is also called the common mode inductor. It is formed by symmetrical winding of two coils with the same number of turns on a closed magnetic ring. The structure is shown in Fig. 8. A common mode choke can also be formed by winding the coaxial line around the magnetic ring, which is shown in Fig. 9. The common mode noise current flows through the two windings in the same direction, and the generated magnetic flux is added in the same direction. The choke exhibits high impedance, thereby suppressing common mode noise. The wires should be close to the magnet, otherwise, it will generate more magnetic leakage and weaken the antiinterference ability. Therefore, the closer the inner diameter of the magnetic ring is to the outer diameter

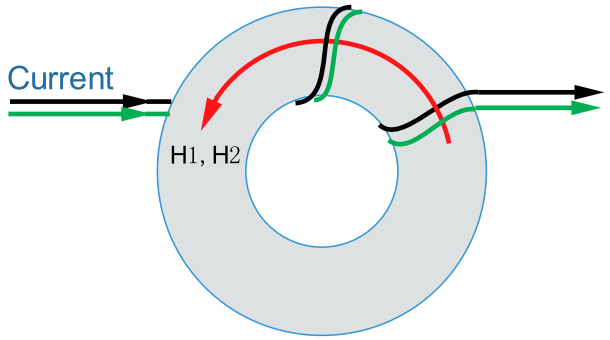

Fig. 9. Two signal lines are wound in parallel on the magnetic ring (two turns in the image) to form a common mode choke. For coaxial lines, the two wires are the core wire and the shield, respectively.

of the wire, the smaller the magnetic leakage, and the better the antiinterference ability. In general, for the magnetic ring of the same material, the inner radius and outer radius of the magnetic ring have a larger difference, and the longer the axial direction, the better is the EMI suppression effect. The ideal common mode choke has only common mode inductance characteristics. In theory, the higher the frequency, the stronger is the suppression effect of the choke. The more the number of turns of the signal wires around the magnetic ring, the stronger the suppression effect. In fact, the inductor will also have a parasitic capacitance in parallel. When the frequency is high, the equivalent resistance of the parasitic capacitance becomes smaller, resulting in the decrease of the equivalent resistance of the choke. The more the number of turns of the signal wire around the magnetic ring, the stronger is the suppression of the low frequency, but the suppression of high frequency is weakened due to the existence of parasitic capacitance.

By using the magnetic rings at one end or both ends of the coaxial line, we can suppress the interference and improve the accuracy of power monitoring and the effectiveness of RF protection. When the magnetic ring was used near the detector, the interference voltage caused by ICRH is about 0.12 V. When the magnetic ring was used near the amplifier, the interference voltage caused by ICRH is about 0.18 V. When two magnetic rings were used at both ends of the coaxial line, the interference voltage caused by ICRH is about 0.03 V. Obviously, it would be better to use two magnetic rings. It also proves that the RF interference signals are transmitted to the detectors through the coaxial lines.

IV. Electromagnetic Compatibility in the Interlock and Overcurrent Protection System

The interlock system and the overcurrent protection system are very important for the safety of the gyrotrons. The influence of the EMI on the interlock and protection system must be analyzed and removed to ensure its stability and effectiveness.

The current transformers are susceptible to the magnetic field [14]. We simulated the influence of the magnetic field strength on the current transformers using the Finite Integration method [15]. Placing the current transformers at a suitable distance from the superconducting magnet can ensure the normal operation of the current transformers. The overcurrent protection circuits were enclosed in the shielded chassis to ensure proper operation of the protection system.

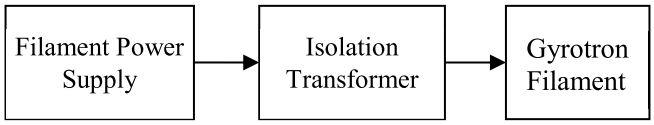

Fig. 10. Connection between the power supply and the gyrotron filament.

The current transformer (model no. 2–0.1 W) from "Stannies Industries" was used to measure the filament primary current for the programmable logic controller (PLC) interlock. The transformers' parameters and their location are similar to the current transformers that measure beam current and anode current [9]. All the current transformers are susceptible to the magnetic field. The influence of the magnetic field on the current transformer has been found in the filament power supply test.

The connection between the filament power supply and the gyrotron filament is shown in Fig. 10. Before we can turn on the filament power supply, we need to open the water cooling system, oil cooling system, magnet power supply (and the magnet current must be greater than 30 A for #1 gyrotron), ion pump power supply, and collector power supply. We gradually increase the filament current, and the test results are shown in Table I. All the data recorded in Table I are the reading just after adjusting the current set value on the panel. After the setting is completed, the filament side (secondary side) current and the secondary side voltage will gradually change with the change of the filament resistance.

The primary current is read by the microampere meter on the panel of the filament power supply, and the secondary current is measured by connecting a 1.986-mΩ resistor in series. The secondary voltage is measured using a multimeter. The primary voltage measurement of PLC is to directly connect the primary side voltage to "0–300-V ac voltage to 4–20-mA dc current" conversion equipment, and the dc current signal is connected to the PLC device. The above measurement methods are relatively accurate. The primary current measurement of PLC is to use the current transformer (Model No. 2–0.1 W).

During the test, the magnet current is gradually increased from 30 to 50.45 A, and the magnetic field strength is gradually increased. The current transformer is located about 1.3 m below the magnet from the center of the magnet, where the maximum magnetic induction is about 0.03 T. The effect of the external magnetic field on the magnetic core easily saturates the magnetic core, resulting in inaccurate measurement results. Therefore, the accuracy of the current measured by the PLC gradually decreases from the top to the bottom in Table I. Considering that the isolation transformer will consume part of the power, the product of the actual primary voltage and current should be slightly larger than the product of the secondary voltage and current, but the measurement results in Table I are not the same. When the measured current of the PLC is about 14 A, the environmental magnetic field generated by the magnet has saturated the core of the current sensor, and the measurement result cannot reflect the actual

TABLE I
TEST RESULTS FOR CFPS 30/50 FILAMENT POWER SUPPLY IN LOCAL FRONT PANEL OPERATION MODE

Primary current displayed on the panel [Arms]	Secondary voltage [Vrms]	Secondary current [A]	Primary voltage measured by PLC [V]	Primary current measured by PLC [A]
1.25	0.588	4.783	1.2	4.2
2.5	0.87	7.553	1.5	5.6
3.75	1.5	9.265	2.2	6.7
5	2.6	10.070	2.7	7.6
6.25	3.4	10.775	3.4	8.3
7.5	4.2	11.480	3.9	8.8
8.75	5.2	12.538	4.8	9.4
10	6	13.343	5.4	9.9
11.25	6.99	14.350	6.4	10.3
12.5	7.8	15.206	7	10.7
13.75	8.9	16.264	7.8	11.2
15	9.9	17.321	8.9	11.6
16.25	11	18.328	9.5	12
17.5	12.1	19.335	10.8	12.3
18.75	13.2	20.342	11.7	12.6
20	14.35	21.349	12.5	12.9
21.25	15.8	22.407	14	13.1
22.5	17.2	23.515	15.1	13.4
23.75	18.5	24.522	17.1	13.6
25	19.9	25.529	19.1	13.7
26.25	22	26.939	21.7	13.9
27.5	23.8	28.248	24	14
28.75	25.8	29.507	25.3	14.2
30	27.84	30.967	25.2	14.33
31.25	30.43	32.326	24.4	14.13
32.5	33.86	34.240	24	14.1
32.5	34.05	33.988	24	14.03
31.25	32.25	32.880	24.3	14.03
30	29.29	31.118	25.2	14.16

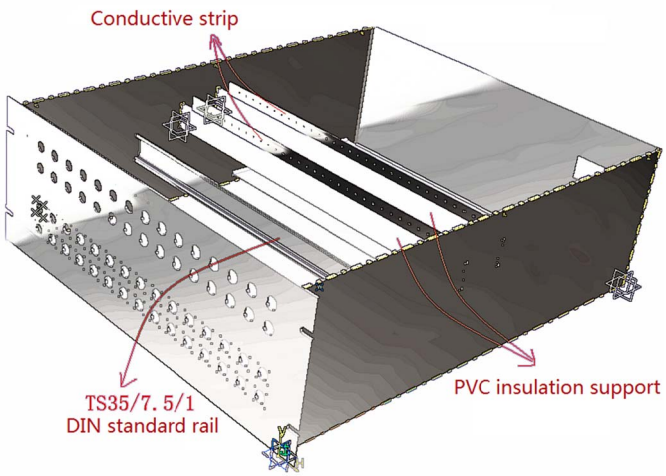

Fig. 11. Isolator chassis structure. The conductive strip is embedded on the insulation support, and the conductive strip has many binding posts.

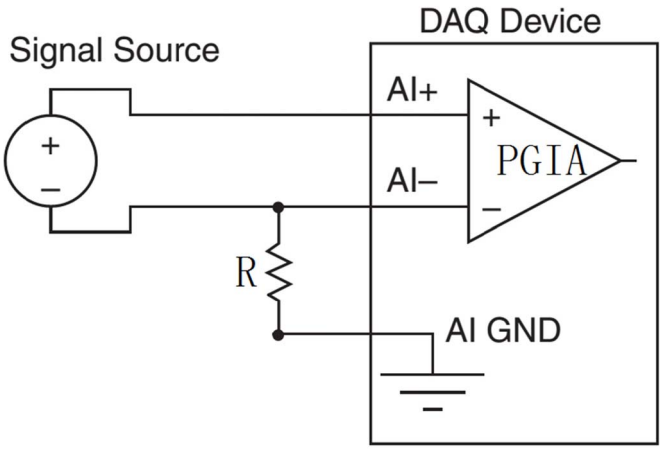

Fig. 12. Pull-down resistor ($R = 100$ kΩ) is connected to the negative signal input port.

current value at all. After we put the current transformers at a distance >2.2 m from the magnet center, the current measured by the PLC became correct.

V. ELECTROMAGNETIC COMPATIBILITY IN THE DAQ SYSTEM

The DAQ system [16] is used to acquire and record gyrotron related signals such as cathode voltage, cathode current, and magnet current. In order to ensure the safety of the acquisition system and reduce the interference of ground bounce and other interference on the signals, we use the isolators to isolate the acquisition cards from the sensors. The isolators used for temperature and flow signal input 4–20 mA two-wire current, output 0–10-V voltage, with a response time of 100 μs; the isolators used for voltage, current and power signals input 0–10-V voltage, output 0–10-V voltage, with a response time of 20 μs.

Because each isolator has only one signal channel and all of them need 24-V power supply, we designed the chassis that is shown in Fig. 11 to integrate the isolators for the convenience of use. Considering that the power consumption of the isolator is low (less than 1 W), in order to better shield the effect and to reduce the complexity and cost, the 2-mm-thick steel plate without cooling holes was used as the casing. Designed as a standard 4U chassis, it can be placed in a 19-in standard rack with a TS35/7.5/1 DIN rail inside for isolator mounting. In actual use, the isolators did not have any EMI problems.

The NI 6229 cards are used for the DAQ. The acquisition card has three acquisition modes: reference single-ended (RSE) mode, differential mode, and nonreference single-ended (NRSE) mode [17]. The differential mode was selected as the DAQ mode due to the bad electromagnetic noise environment around the signal lines. Because the isolators output floating signals, the pull-down resistors need to be connected to the signal input ports to provide the return paths for the input differential amplifiers of the acquisition cards. As shown in Fig. 12, only one pull-down resistor ($R = 100$ kΩ) was used to connect the negative signal input port in our system because the isolator usually outputs a positive voltage signal. The reason why it is connected to the ground through a resistor is to balance the noise between the two input signals of the differential amplifier, so that the noise signals input from the two input terminals are as equal as possible. This configuration does not pull down the amplifier input impedance.

In the above configuration, all signals can be acquired normally, except the #2 anode voltage signal. No. 2 anode voltage is sent through the other photoelectric isolation device.

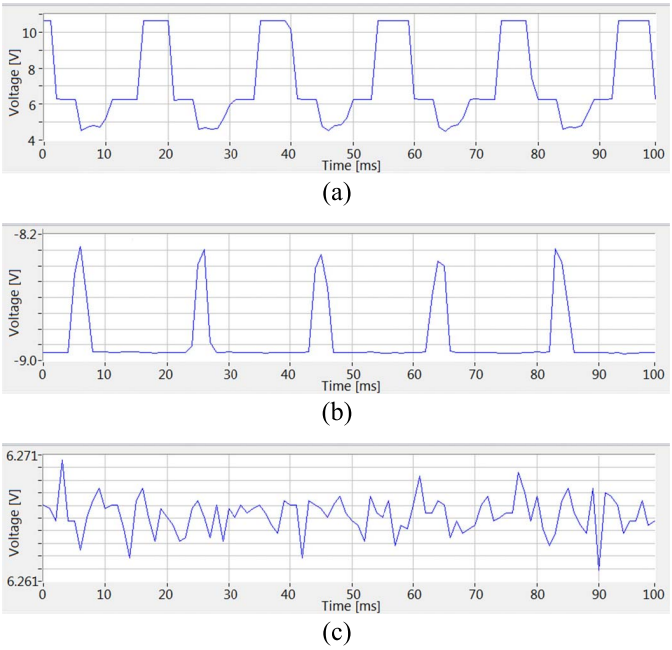

Fig. 13. Acquired waveforms of #2 anode voltage when use (a) differential mode, (b) NRSE mode, and (c) RSE mode.

When the differential mode (a 100-kΩ pull-down resistor is connected to the negative signal input port) or the NRSE mode selected, the DAQ card acquired the wrong data. When the RSE mode is selected, the acquired waveform is normal, which is shown in Fig. 13.

The reason why this signal can not be acquired normally is that the anode voltage output by the photoelectric isolator may have an occasional negative value. When the signal is negative, there is no current return path, resulting in an abnormal signal. The solutions are as follows.

1) Differential acquisition is still used, and the 100-kΩ pull-down resistor must be connected to both the positive and negative terminals of the amplifier. This will cause the input resistance of the DAQ card to change from 10 GΩ to 200 kΩ [17].
2) Use RSE mode.

Using the first method results in reduced input impedance, which in turn reduces the accuracy of the acquisition. Considering that the length of the signal line does not exceed 1 m, the EMI that may be introduced is not large; the RSE acquisition mode was selected.

In addition to the above signal problems, the temperature transmitters are also susceptible to the EMI. We use the temperature transmitter to measure the water temperature of each water-cooling branch. The platinum resistance was used as the temperature sensor. The temperature transmitter outputs a 4–20-mA signal, which is proportional to the temperature of 0 °C–100 °C. The reason why the platinum resistance sensor is chosen instead of the thermocouple is that the former has higher precision.

Fig. 14 shows that the temperature transmitter on the #1 dummy load branch is affected by the EMI. We found that the interference disappeared after separating the temperature transmitter from the water pipe. The methods of adding

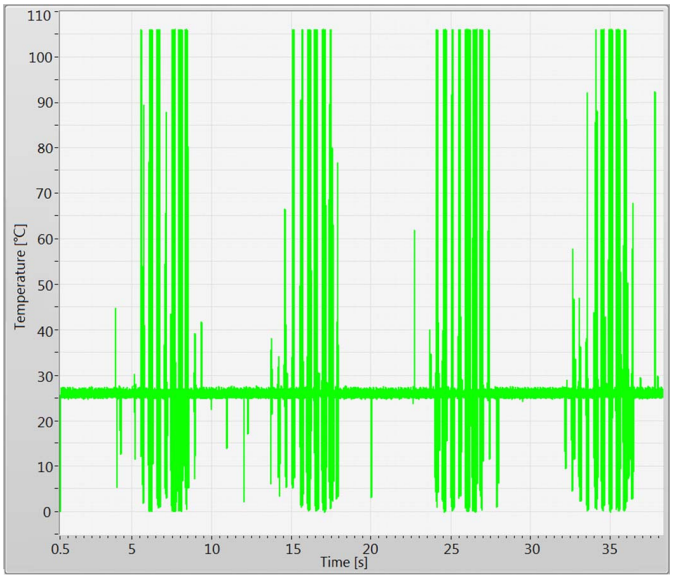

Fig. 14. Temperature transmitter on the #1 dummy load branch is affected by the EMI.

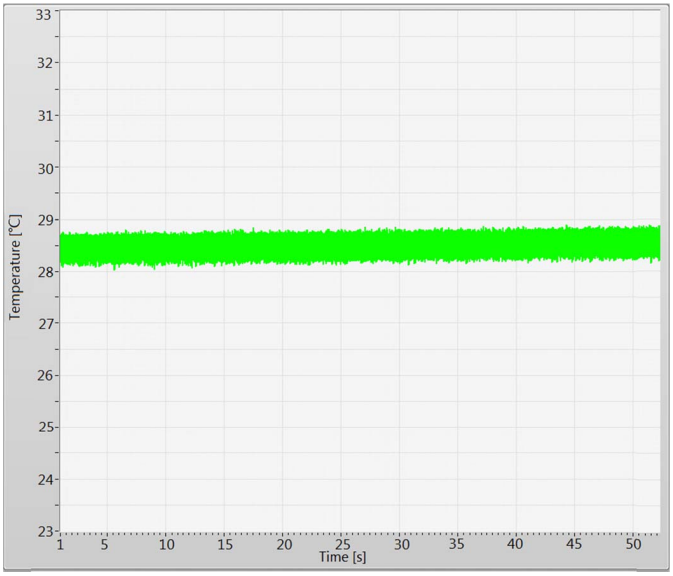

Fig. 15. Interference was gone after we changed a better shielded twisted pair.

the magnetic ring and the grounding of the shielding layer are invalid, and the interference is still present. Probably because the shielding of the twisted pair is poor, resulting in the common mode interference of the temperature signal. As expected, after we changed the better shielded twisted pair, the interference was gone, which is shown in Fig. 15.

VI. Conclusion

The ECRH system is a complex terahertz system. In the development and operation of the EAST ECRH system, we have found many electromagnetic compatibility problems in the system. These electromagnetic compatibility problems have been analyzed, tested, and resolved, which were discussed in this paper.

The RF protection system is an important subsystem for gyrotrons to realize the RF protection and to monitor the wave power in real time. The EMI seriously affects the system security. By calculation and analysis, we found that the RF interference signals are transmitted to the detectors through the coaxial lines. By using the magnetic rings at both ends of the coaxial lines, we can better suppress the interference and improve the accuracy of power monitoring and the effectiveness of RF protection. The current transformers are used to realize the overcurrent protection, which are liable to be influenced by the magnetic field. Placing the current transformers at a suitable distance from the superconducting magnet can ensure the normal operation of the current transformers. The isolators are used in the DAQ system. Because the isolators output floating signals, the pull-down resistors were connected to the signal input ports to provide the return paths for the input differential amplifiers of the acquisition cards. The effect of EMI on the temperature transmitter was also found and resolved. After solving all the above electromagnetic compatibility problems, the ECRH system can stably output high-power terahertz waves.

REFERENCES

[1] J. Li *et al.*, "A long-pulse high-confinement plasma regime in the experimental advanced superconducting tokamak," *Nature Phys.*, vol. 9, pp. 817–821, Nov. 2013.

[2] J. S. Hu *et al.*, "New steady-state quiescent high-confinement plasma in an experimental advanced superconducting tokamak," *Phys. Rev. Lett.*, vol. 114, no. 5, p. 055001, 2015.

[3] M. Henderson *et al.*, "The targeted heating and current drive applications for the ITER electron cyclotron system," *Phys. Plasmas*, vol. 22, pp. 021808-1–021808-15, Feb. 2015.

[4] G. Dammertz *et al.*, "Development of a 140-GHz 1-MW continuous wave gyrotron for the W7-X stellarator," *IEEE Trans. Plasma Sci.*, vol. 30, no. 3, pp. 808–818, Jun. 2002.

[5] D. S. Tax, O. V. Sinitsyn, W. C. Guss, G. S. Nusinovich, M. A. Shapiro, and R. J. Temkin, "Experimental study of the start-up scenario of a 1.5-MW, 110-GHz gyrotron," *IEEE Trans. Plasma Sci.*, vol. 41, no. 4, pp. 862–871, Apr. 2013.

[6] R. Ikeda *et al.*, "Development of 170 GHz, 1 MW gyrotron with high-order $TE_{31,11}$ mode oscillation for ITER EC system," *Fusion Eng. Design*, vol. 128, pp. 23–27, Mar. 2018.

[7] H. Xu *et al.*, "Development and preliminary commissioning results of a long pulse 140 GHz ECRH system on EAST tokamak (invited)," *Plasma Sci. Technol.*, vol. 18, no. 4, pp. 442–448, 2016.

[8] W. Xu, H. Xu, F. Liu, J. Wang, X. Wang, and Y. Hou, "Calorimetric power measurements in the EAST ECRH system," *Plasma Sci. Technol.*, vol. 19, no. 10, p. 105602, 2017.

[9] M. Cengher *et al.*, "Performance and upgrades for the electron cyclotron heating system on DIII-D," *IEEE Trans. Plasma Sci.*, vol. 42, no. 7, pp. 1964–1970, Jul. 2014.

[10] V. Erckmann *et al.*, "ECRH and W7-X: An intriguing pair," *AIP Conf. Proc.*, vol. 1580, no. 1, pp. 542–545, 2014.

[11] W. Xu *et al.*, "Millimeter wave power monitoring in EAST ECRH system," *IEEE Access*, vol. 4, no. 1, pp. 5809–5817, 2016.

[12] F. K. Liu *et al.*, "First results of LHCD experiments with 4.6 GHz system toward steady-state plasma in EAST," *Nucl. Fusion*, vol. 55, no. 12, p. 123022, 2015.

[13] X. Zhang *et al.*, "Current status of ICRF heating experiments on EAST," *Plasma Sci. Technol.*, vol. 13, no. 2, p. 172, 2011.

[14] W. Xu *et al.*, "Overcurrent protection for gyrotrons on the experimental advanced superconducting tokamak," *IET Sci. Meas. Technol.*, vol. 12, no. 6, pp. 726–732, Sep. 2018.

[15] M. Clemens and T. Weiland, "Discrete electromagnetism with the finite integration technique," *Prog. Electromagn. Res.*, vol. 32, pp. 65–87, 2001

[16] W. Xu, H. Xu, F. Liu, F. Hou, and Z. Wu, "Data acquisition system for electron cyclotron resonance heating on EAST tokamak," *Fusion Eng. Design*, vol. 113, pp. 119–125, Dec. 2016.

[17] *DAQ M Series M Series User Manual*, Nat. Instrum., Austin, TX, USA, Jul. 2008.

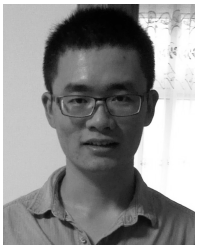

Weiye Xu (M'–) was born in Qufu, Shandong, China, in 1990. He received the B.S. degree in electronic science and technology from Shandong Normal University, Jinan, Shandong, China, in 2011, and the Ph.D. degree in nuclear energy science and engineering from the University of Chinese Academy of Sciences, Beijing, China, in 2017.

He is currently an Assistant Professor with the Institute of Plasma Physics, Chinese Academy of Sciences, Hefei, Anhui, China. His current research interests include the high-power microwave heating technology for plasma, electronic technology, electromagnetic field theory, and microwave technology.

Handong Xu was born in Yuexi county, Anhui, China. He received the M.S. degree in microwave engineering from the Institute of Plasma Physics, Chinese Academy of Sciences, Hefei, China, in 2004, and the Ph.D. degree in advanced energy engineering from Kyushu University, Fukuoka, Japan, in 2008.

He participated in the research of 4-MW 2.45-GHz and 6-MW 4.6-GHz lower hybrid current drive on EAST from 2009 to 2011. Since 2012, he has been studying 140-GHz 4-MW electron cyclotron resonance heating (ECRH) system and ECRH experiments on EAST. He is currently a Professor with the Institute of Plasma Physics, Chinese Academy of Sciences. His current research interests include the development of high-power microwave heating and current drive system and corresponding experiment study on EAST Tokamak devices.

Fukun Liu is currently a Professor at the Institute of Plasma Physics, Chinese Academy of Sciences, Hefei, Anhui, China. His current research interests include microwave technology and experimental plasma physics.

Huaichuan Hu is currently with the Institute of Plasma Physics, Chinese Academy of Sciences, Hefei, Anhui, China. His current research interests include klystron operation and interlock system design.

Jianqiang Feng is currently with the Institute of Plasma Physics, Chinese Academy of Sciences, Hefei, Anhui, China. His current research interests include electronic technology and so on.